IEEE Access
Multidisciplinary | Rapid Review | Open Access Journal

Received June 25, 2020, accepted July 16, 2020, date of publication July 21, 2020, date of current version July 30, 2020.

Digital Object Identifier 10.1109/ACCESS.2020.3010835

A Novel Chip Pulse Employed by Ranging Code Based on Simultaneous Transmitting CPM Modulation and PN Ranging in Inter-Satellite Links of GNSS

RUI XUE[1], TONG WANG[1], AND HUAIYU TANG[2]
[1]College of Information and Communication Engineering, Harbin Engineering University, Harbin 150001, China
[2]China Research Institute of Radiowave Propagation, Xinxiang 453000, China

Corresponding author: Tong Wang (wangtong736@hotmail.com)

This work was supported in part by the National Natural Science Foundation of China under Grant 61873070, in part by the Technology Development Project of the China Research Institute of Radiowave Propagation under Grant JW2019-114, and in part by the Heilongjiang Province Key Laboratory of High Accuracy Satellite Navigation and Marine Application Laboratory under Grant HKL-2020-Y03.

ABSTRACT The construction of a navigation constellation with inter-satellite links (ISLs) has become one of the important development trends for new-generation global navigation satellite systems (GNSSs), and ISLs currently realize navigation and communication functions through separate low-rate omnidirectional telemetry, tracking, command and high-rate data service channels, respectively. If the above two functions are integrated into one channel, this will result in simplification of the onboard equipment, improvement of the electromagnetic compatibility, power consumption reduction and frequency resources savings, and we speculate that autonomous navigation will be achieved by ISLs with navigation and communication fusion. In this paper, a system capable of simultaneous high-data rate communication transmission and precision ranging is investigated, and a specific scheme is introduced by combining continuous phase modulation (CPM) and a pseudonoise (PN) ranging code denoted as CPM + PN. The chip pulse is one of the key factors to design the ranging code, which not only affects the ranging performance but also influences the properties of the CPM + PN scheme, such as its spectral characteristics, communication reliability, and acquisition time. To consider the above performance indexes, a new chip pulse based on a normally distributed wave is proposed. Theoretical analysis and simulation results show that compared to square-wave and half-sine wave cases, the normally distributed wave attains great advantages in the ranging accuracy and communication reliability, which become more notable with reasonable selection of the energy distribution index. Moreover, the proposed chip pulse achieves a similar acquisition time as the traditional wave. As a result, the normally distributed wave can be used as a better alternative to the ranging chip pulse for the CPM + PN waveform.

INDEX TERMS GNSS, ISLs, CPM + PN, chip pulse, normally distributed.

I. INTRODUCTION

Inter-satellite links (ISLs) can be used as a bridge between navigation satellites to connect the satellites as a whole and form a three-dimensional crossover network through mutual communication and ranging [1], [2]. ISLs can shorten the update cycle of ephemeris, realize joint-orbit determination of the navigation constellation, and notably improve the orbit determination accuracy [3]; Moreover, ISLs improve the integrity of a global navigation satellite system (GNSS) by providing an independent means to assess ephemeris and clock parameters. The establishment of ISLs enables the navigation constellation to attain a short routing delay and high communication capacity, which can considerably improve the measurement and control performance of the satellite navigation system [4]. Therefore, ISLs been a key technology to realize autonomous navigation (without the support of ground stations) for the new generation of GNSSs [5], [6].

GNSSs generally adopt the standard telemetry, tracking, command system and spectrum range to transmit

The associate editor coordinating the review of this manuscript and approving it for publication was Masood Ur-Rehman.

low-code rate ranging data, and employ binary-phase shift keying (BPSK) and quadrature-phase shift keying (QPSK) systems to transmit high-code rate communication information [7]. Ranging and communication signals are transmitted through two independent channels, which require not only a large bandwidth but also two sets of transmitters and receivers. In reference [8], the unbalanced QPSK system is adopted to transmit high and low bit rate data simultaneously, in which the same-phase branch is applied to transmit the communication data and the orthogonal branch is used to transmit the ranging data. However, it achieves a low bandwidth efficiency and when the communication bit rate is higher than 2 Mbit per second (Mbps), it cannot meet the constraint requirements of the space frequency coordination group (SFCG) across the spatial spectrum [9], [10].

To satisfy the demand for the simultaneous transmission of high-bit rate communication and ranging data signals, the National Aeronautics and Space Administration (NASA) combined the Gaussian-filtered minimum shift keying (GMSK) system with a pseudonoise (PN) code and proposed a new information transmission system, which can be expressed as GMSK + PN [11], [12]. When the communication bit rate is higher than 2 Mbps, GMSK + PN signals can still meet the SFCG requirements. The information transmission system is favored by the Consultative Committee for Space Data System (CCSDS) and the European Space Agency (ESA) [13]–[18] and has become an area of increased interest in CCSDS and ESA seminars in recent years.

The main sources of interference between communication and regenerative PN code ranging include the selection of the communication modulation signal, data rate of communication, ranging modulation index, ranging code, ranging code forming filter and ranging code rate [19]. Similar to GMSK, multi-h continuous phase modulation (multi-h CPM) has the advantages of a continuous phase, constant envelope and high spectrum utilization [20], [21]. In addition, multi-h CPM attains a greater flexibility [22] and can choose the appropriate shaping pulse function, modulation index and modulation order according to the system requirements for a suitable spectrum efficiency and error code performance [23], [24]. Multi-h CPM is also suitable for the multiband combined navigation approach in future high-precision positioning navigation systems [25]. Therefore, this paper chooses multi-h CPM for the communication modulation signal of the system that combines communication with ranging. In terms of the ranging code, chaotic sequences achieve a superior performance, but only for square waves [26], [27]. In the CCSDS standard, the PN ranging code called Weighted-voting balanced Tausworthe, $v = 2$ (T2B) is recommended for low signal-to-noise links because of its shorter acquisition time, while the Weighted-voting balanced Tausworthe, $v = 4$ (T4B) is recommended for high ranging accuracy cases [28]. Therefore, we mainly consider the above two kinds of ranging sequences in this paper.

The PN ranging chip pulse imposes a great influence on the communication bit error rate (BER) and ranging accuracy. However, most studies on the chip pulse only focus on square and sine waves [29]–[31]. The performance of these two waves is not ideal when the required ranging accuracy is high. In addition, these two waves will cause a greater interference to the communication signal, which will result in a reduced reliability and the disadvantage becomes more notable when the proportion of the ranging component is large. This paper conducts an in-depth analysis of this problem and focuses on jitter error reduction in the code tracking loop. Finally, a normally distributed wave with a high accuracy and reliability is designed.

The rest of this paper is organized as follows. Section II introduces the system model of the CPM + PN transmitter and receiver. Section III analyzes the factors that impact the ranging performance. Section IV designs the chip pulse based on the normally distributed wave. Section V provides the simulation results of the designed and traditional waves. Finally, we conclude the paper in Section VI.

II. SYSTEM MODEL OF THE CPM + PN SCHEME

A block diagram of the CPM + PN transmitter is shown in Figure 1. A low-density parity check (LDPC) encoder, shaping filter and integrator are adopted for the communication input stream to generate the CPM communication phase, while the PN ranging sequence passes through the shaping filter and is multiplied with the weighting factor to obtain the PN ranging phase. After the communication phase and ranging phase are acquired, phase modulation is performed to obtain the CPM + PN composite signal.

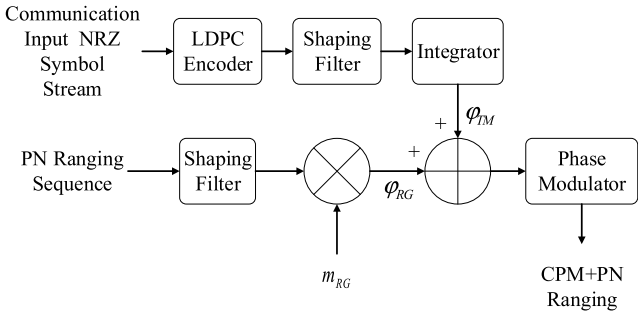

FIGURE 1. CPM + PN transmitter.

The CPM + PN composite signal at the output of the transmitter can be described as:

$$s(t) = \sqrt{2P_T}\cos\left[\omega_s t + \varphi_{TM}(t) + \varphi_{RG}(t)\right] \tag{1}$$

where P_T is the transmission power (W), ω_s is the carrier frequency (rad/s), $\varphi_{TM}(t)$ is the phase of the CPM signal with symbol interval $T_s = 1/R_{TM}$ (s), R_{TM} is the communication symbol rate (symbol/s), and $\varphi_{TM}(t)$ can be written as:

$$\varphi_{TM} = 2\pi h_{CPM}\sum_{i=0}^{n}\alpha_i q(t - iT_s), \quad nT_s \le t \le (n+1)T_s \tag{2}$$

where $h_{CPM} = K/P$ is the CPM modulation index, K and P are the co-prime, $\alpha_i (0 \le i \le n)$ is the M-ary communication

information sequence, and $q(t)$ is a continuous monotone function and can be expressed as:

$$q(t) = \begin{cases} 0 & t \le 0 \\ 1/2 & t > LT_s \end{cases} \tag{3}$$

The phase pulse can be obtained by integrating the rectangular pulse (LREC) with a duration of LT_s, the raised cosine pulse (LRC) or the GMSK pulse and can be expressed as $q(t) = \int_{-\infty}^{t} g(\tau)$, where $g(t)$ is the pulse shaping function.

$\varphi_{RG}(t)$ is the phase of the PN ranging signal and can be described as:

$$\varphi_{RG}(t) = m_{RG} \sum_{n} c_n h(t - nT_c) \tag{4}$$

where $m_{RG} = \pi h/2$ is the peak PN ranging modulation index in radians (without a subcarrier) and the value of h is set to 0.1, 0.2, etc. to control the division of power between the communication and ranging signals, and the power can be described as:

$$P_{TM} = P_T J_0^2(m_{RG}) \quad P_{RG} = P_T 2J_1^2(m_{RG}) \tag{5}$$

where $J_n(\cdot)$ is the standard Bessel function.

Figure 2 shows the power variation trend of the communication and ranging signals with h (the transmission power P_T is assumed to be 1). The value of h determines the communication demodulation performance and ranging accuracy to a certain extent. Simulations [32] with real communication and ranging synchronizers have shown that the system operates as long as h is maintained between 0.1 (favoring communication) and 0.2 (favoring ranging).

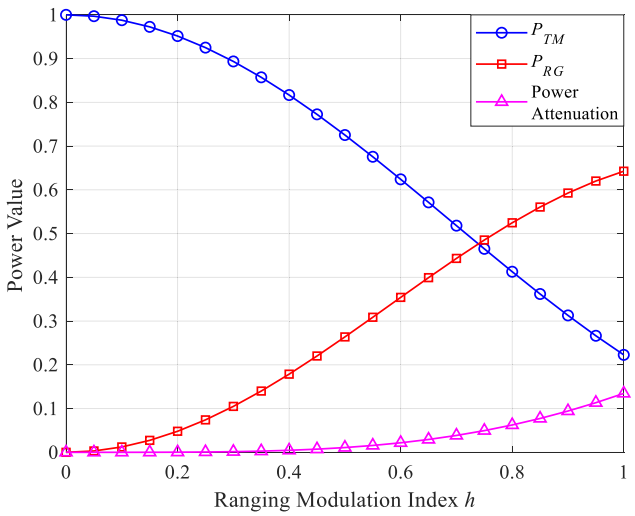

FIGURE 2. Power variation trend of the communication and ranging signals.

The pseudorandom binary sequence $c_n = \pm 1$ is selected in terms of T2B and T4B according to the recommendations of the CCSDS standard, where $h(t - nT_c)$ is the PN ranging shaping filter impulse response (square wave, half-sine wave, etc.), $T_c = 1/R_{RG}$ is the PN ranging chip interval, and R_{RG} is the ranging chip rate (chip/s).

With the use of familiar trigonometric identities equation (1) can be decomposed into:

$$\begin{aligned} s(t) &= \sqrt{2P_T}\cos\left[\omega_s t + \varphi_{TM}(t) + \varphi_{RG}(t)\right] \\ &= \sqrt{2P_T}\cos\left[\omega_s t + \varphi_{TM}(t) + m_{RG}c_n h(t)\right] \\ &= \sqrt{2P_T}\left[Q(t)\cos(\omega_s t) - I(t)\sin(\omega_s t)\right] \end{aligned} \tag{6}$$

where

$$\begin{aligned} I(t) &= \sin[\varphi_{TM}(t) + m_{RG}c_n h(t)] \\ &= \sin[\varphi_{TM}(t)]\cos[m_{RG}c_n h(t)] \\ &\quad + \cos[\varphi_{TM}(t)]\sin[m_{RG}c_n h(t)] \end{aligned} \tag{7}$$

$$\begin{aligned} Q(t) &= \cos[\varphi_{TM}(t) + m_{RG}c_n h(t)] \\ &= \cos[\varphi_{TM}(t)]\cos[m_{RG}c_n h(t)] \\ &\quad - \sin[\varphi_{TM}(t)]\sin[m_{RG}c_n h(t)] \end{aligned} \tag{8}$$

Since $c_n = \pm 1$, equations (7) and (8) can be simplified as:

$$\begin{aligned} I(t) &= \sin[\varphi_{TM}(t)]\cos[m_{RG}h(t)] \\ &\quad + c_n\cos[\varphi_{TM}(t)]\sin[m_{RG}h(t)] \end{aligned} \tag{9}$$

$$\begin{aligned} Q(t) &= \cos[\varphi_{TM}(t)]\cos[m_{RG}h(t)] \\ &\quad - c_n\sin[\varphi_{TM}(t)]\sin[m_{RG}h(t)] \end{aligned} \tag{10}$$

A block diagram of the CPM + PN receiver is shown in Figure 3. The received signal can be passed directly to the CPM demodulator whereby the ranging signal is regarded as noise, and it then passes through the LDPC encoder, shaping filter and FM modulator to obtain the regenerative communication signal. Via the removal of the regenerative communication information from the received signal, the PN ranging information is reproduced.

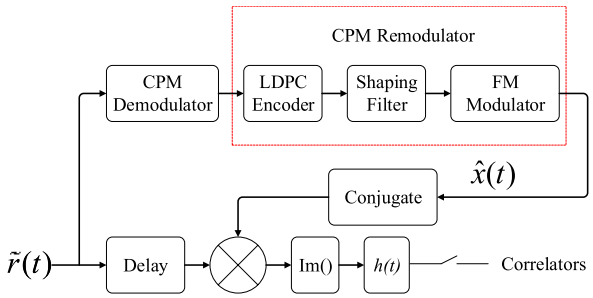

FIGURE 3. CPM + PN receiver.

The complex envelope of the received signal can be expressed as:

$$\tilde{r}(t) = \sqrt{2P_T}\exp[j\varphi_{TM}(t) + j\varphi_{RG}(t)] + n(t) \tag{11}$$

where $n(t)$ is the noise. The regenerative communication signal can be expressed as:

$$\hat{x}(t) = \exp[j\hat{\varphi}_{TM}(t)] \tag{12}$$

Multiple correlation analysis between the received signal and regenerative communication signal is conducted to generate

the signal as:

$$\begin{aligned} z(t) &= \tilde{r}(t)\hat{x}^*(t) \\ &= \sqrt{2P_T}\exp[j\varphi_{TM}(t) + j\varphi_{RG}(t) - j\hat{\varphi}_{TM}(t)] + n(t) \\ &\approx \sqrt{2P_T}\exp[j\varphi_{RG}(t)] + n(t) \end{aligned} \tag{13}$$

The phase of the PN ranging signal can be obtained by determining the imaginary part after Taylor approximation of equation (13):

$$\begin{aligned} \mathrm{Im}\{z(t)\} &= \mathrm{Im}\left\{\sqrt{2P_T}[1 + j\varphi_{RG}(t)]\right\} + n(t) \\ &= \sqrt{2P_T}\varphi_{RG}(t) \end{aligned} \tag{14}$$

III. RANGING PERFORMANCE ASSESSMENT

The CPM + PN scheme is mainly evaluated from the power spectrum, communication reliability, ranging acquisition time and ranging jitter error. The power spectrum and communication reliability are analyzed from the simulation results in section V. The acquisition time and jitter error are derived in the rest of this section.

A. ACQUISITION TIME

References [11] and [12] have studied the evaluation of the acquisition time for different PN ranging sequences. When the communication signal is absent, the number of correlation chips N_{chip} can be calculated as:

$$N_{chip} = \frac{\eta}{E_{RG}/N_0} = \frac{\eta}{erf^{-1}(1 - 2CER)} \tag{15}$$

where E_{RG} is the ranging chip energy, N_0 is the noise power spectral density of the additive Gaussian noise, CER is the chip error rate, and η is equal to 4305.3 for T4B and 261.2 for T2B.

In the ideal case (communication and ranging signals are both transmitted, but there is no interference between them and the two signals are orthogonal), the chip error rate CER can be replaced by [33]:

$$CER = \frac{1}{2}erfc\sqrt{\frac{E_{RG}}{N_0}} = \frac{1}{2}erfc\sqrt{\frac{P_{RG}}{N_0 R_{RG}}} \tag{16}$$

According to the power relationship in equation (5), the chip energy-to-noise ratio E_{RG}/N_0 can be derived as:

$$\begin{aligned} \frac{E_{RG}}{N_0} &= \frac{P_{RG}}{N_0 R_{RG}} = \frac{2J_1^2(m_{RG})P_T}{N_0 R_{RG}} \\ &= \frac{2J_1^2(m_{RG})}{J_0^2(m_{RG})}\frac{P_{TM}}{N_0 R_{RG}} = \frac{2J_1^2(m_{RG})}{J_0^2(m_{RG})}\frac{R_b}{R_{RG}}\frac{E_b}{N_0} \end{aligned} \tag{17}$$

where E_b is the energy per communication bit, and R_b is the communication bit rate (bit/s). The acquisition time can be thus determined as:

$$\begin{aligned} t_{obs} &= N_{chip}T_c = \frac{J_0^2(m_{RG})}{2J_1^2(m_{RG})}\frac{R_{RG}}{R_b}\frac{T_c\eta}{E_b/N_0} \\ &= \frac{J_0^2(m_{RG})}{2J_1^2(m_{RG})}\frac{1}{R_b}\frac{\eta}{E_b/N_0} \end{aligned} \tag{18}$$

Equation (18) can be implemented to estimate the acquisition time from the measured E_b/N_0 value when the communication signal is present, and E_b/N_0 must be set to acquire the target BER.

B. RANGING JITTER

The designed code tracking loop (CTL) is the key module of the ranging receiver, which determines the range accuracy to a great extent. The CTL block diagram can be designed as shown in Figure 4. The mid-phase integrator represents a solution that estimates the phase error of the CTL input signal. The ±1 alternate sequence is implemented instead of the in-phase integral branch (including the transition detector) considering that PN ranging code sequences with notable clock components can be regarded as a square-wave with a few errors. The output of the mid-phase integrator is multiplied by the ±1 alternate sequence to provide the right CTL correction. The chip rate is obtained by adding the carrier loop error to the nominal chip rate and is adopted to control the numerically controlled oscillator (NCO) frequency.

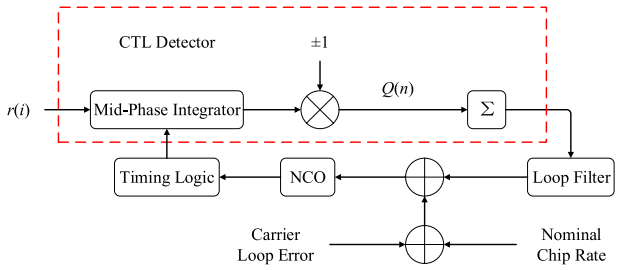

FIGURE 4. CTL block diagram.

The input signal of the CTL can be defined as:

$$r(i) = r(it_s) = A\sum_n c_n \cdot h(it_s - nT_c - \tau) + N_i \tag{19}$$

where t_s is the sampling interval, A is the amplitude of the chip, c_n is the pseudorandom binary sequence, $h(t)$ is the ranging chip shaping function, T_c is the chip period, τ is the random phase to be estimated, and N_i is the zero-mean white Gaussian noise sample with a variance of $\sigma_i^2 = N_0/2t_s$.

A mid-phase integration diagram is shown in Figure 5. It can be assumed that the input symbols of the CTL change at the leading edge as $\cdots nT_c + \tau, (n+1)T_c + \tau \cdots$, and the tracking loop changes at the leading edge as $\cdots nT_c + \hat{\tau}$, $(n+1)T_c + \hat{\tau} \cdots$. The timing error can be expressed as:

$$\varepsilon = \tau - \hat{\tau} \tag{20}$$

$S(\varepsilon)$ is defined as the mean value of the error control signal conditioned on the timing error and can be described as

$$S(\varepsilon) = L \cdot E(Q_n|\varepsilon) \tag{21}$$

where $E(\cdot)$ is the mathematical expectation, Q_n is the quadrature channel output, and L is the cumulative length of the accumulator after the orthogonal branch.

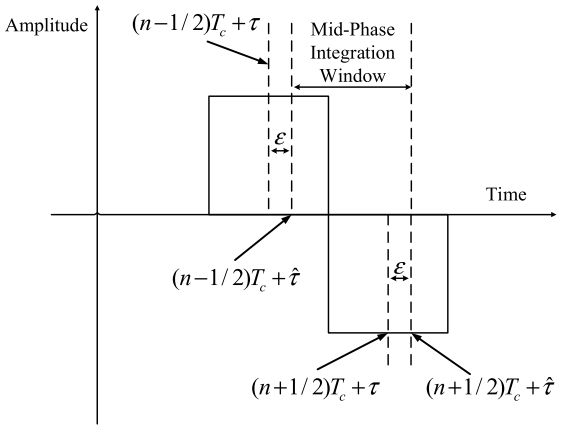

FIGURE 5. Mid-phase integration.

The output of the mid-phase integrator Q_n can be determined as:

$$Q_n = \sum_{i\in C_n} r(i) = \sum_{i\in C_n} \{A[c_n \cdot h(it_s - nT_c - \tau)] + N_i\} \quad (22)$$

where C_n is the collection of:

$$i : \left(n - \frac{1}{2}\right) T_c + \hat{\tau} \le it_s < \left(n + \frac{1}{2}\right) T_c + \hat{\tau} \quad (23)$$

The mean value of Q_n can be calculated as:

$$E(Q_n) = \frac{A \int_{-\varepsilon}^{\varepsilon} h(t + T_c/2)dt}{t_s} \quad (24)$$

It is assumed that the derivative of $H(t)$ is $h(t)$, i.e.:

$$H'(t) = h(t) \quad H'(t + T_c/2) = h(t + T_c/2) \quad (25)$$

The definite integral of $h(t + T_c/2)$ can be calculated as

$$\begin{aligned}\int_{-\varepsilon}^{\varepsilon} h(t + T_c/2)dt &= H(t + T_c/2)|_{-\varepsilon}^{\varepsilon} \\ &= H(\varepsilon + T_c/2) - H(-\varepsilon + T_c/2)\end{aligned} \quad (26)$$

The S curve can be expressed as:

$$\begin{aligned}S(\varepsilon) &= \frac{L \cdot A \int_{-\varepsilon}^{\varepsilon} h(t + T_c/2)dt}{t_s} \\ &= \frac{L \cdot A\,[H(\varepsilon + T_c/2) - H(-\varepsilon + T_c/2)]}{t_s}\end{aligned} \quad (27)$$

The slope of the S curve at the origin represents the CTL gain K_ε:

$$\begin{aligned}K_\varepsilon &= \left.\frac{\partial S(\varepsilon)}{\partial \varepsilon}\right|_{\varepsilon=0} \\ &= \frac{L \cdot A}{t_s} \left.\frac{\partial \left[H\left(\varepsilon + \frac{T_c}{2}\right) - H\left(-\varepsilon + \frac{T_c}{2}\right)\right]}{\partial \varepsilon}\right|_{\varepsilon=0} \\ &= \frac{L \cdot A}{t_s} \left.\left[h\left(\varepsilon + \frac{T_c}{2}\right) + h\left(-\varepsilon + \frac{T_c}{2}\right)\right]\right|_{\varepsilon=0} \\ &= \frac{L \cdot A}{t_s} 2h\left(\frac{T_c}{2}\right)\end{aligned} \quad (28)$$

After L times of accumulation, the variance in the white Gaussian noise at the phase detector output can be defined as:

$$\sigma_N^2 = L\frac{T_c}{t_s}\sigma_i^2 = \frac{LT_cN_0}{2t_s^2} \quad (29)$$

The spectral density of the additive noise in the CTL can be obtained as:

$$S_N = \sigma_N^2 \cdot (L \cdot T_c) = \frac{L^2T_c^2N_0}{2t_s^2} \quad (30)$$

Moreover, the tracking performance of the CTL in terms of the timing jitter σ_ε^2 can be defined as

$$\begin{aligned}\sigma_\varepsilon^2 &= \frac{2B_LS_N}{K_\varepsilon^2} = \frac{B_LL^2T_c^2N_0}{t_s^2}\frac{t_s^2}{4h^2(T_c/2)L^2A^2} \\ &= \frac{1}{4h^2(T_c/2)}\frac{B_LT_c^2}{P_{RG}/N_0}\end{aligned} \quad (31)$$

where B_L is the one-side loop bandwidth, $P_{RG} = A^2$ is the ranging chip power, and P_{RG}/N_0 is the ranging power-to-noise spectral density ratio, which can be converted into (similar to equation (17)):

$$\frac{P_{RG}}{N_0} = \frac{2J_1^2(m_{RG})}{J_0^2(m_{RG})}\frac{E_b}{T_bN_0} \quad (32)$$

where E_b is the energy per communication bit, and T_b is the bit interval.

During the actual operation of the CTL, not all the power of the ranging signal is applied to track the chip rate because of the loop filter, and it is necessary to replace P_{RG} with the ranging clock component. For the ranging codes T2B and T4B, the attenuation of the ranging clock component to the whole composite pseudocode power can be expressed as $L_{ck} = 0.3936$ for T2B and $L_{ck} = 0.881$ for T4B. Therefore, the ranging timing jitter (seconds) can be determined as:

$$\begin{aligned}\sigma_\varepsilon &= \frac{T_c}{2h(T_c/2)}\sqrt{\frac{B_L}{L_{ck} \cdot P_{RG}/N_0}} \\ &= \frac{T_c}{2h(T_c/2)}\frac{J_0(m_{RG})}{J_1(m_{RG})}\sqrt{\frac{B_LT_b}{2L_{ck}}\frac{1}{E_b/N_0}}\end{aligned} \quad (33)$$

where E_b/N_0 must satisfy the target BER constraint. Finally, the one-way ranging jitter (meters) can be written as:

$$\sigma = \frac{c}{2}\sigma_\varepsilon = \frac{cT_c}{4h(T_c/2)}\frac{J_0(m_{RG})}{J_1(m_{RG})}\sqrt{\frac{B_LT_b}{2L_{ck}}\frac{1}{E_b/N_0}} \quad (34)$$

where c is the speed of light.

Equation (34) indicates that the ranging jitter is mainly related to the center peak of the chip pulse, ranging modulation index, tracking loop bandwidth, ranging code sequence and channel condition. In terms of the ranging chip pulse, the higher the central peak is, the smaller the ranging jitter error is.

IV. RANGING CHIP PULSE DESIGN

The traditional ranging chip pulse mainly includes the square wave (sq), half-sine wave (sin) and time domain-rising cosine wave (tdrc):

$$h_{sq}(t) = \begin{cases} 1 & t = [0, T_c] \\ 0 & otherwise \end{cases} \tag{35}$$

$$h_{\sin}(t) = \begin{cases} \sqrt{2}\sin(\pi t/T_c) & t = [0, T_c] \\ 0 & otherwise \end{cases} \tag{36}$$

$$h_{tdrc}(t) = \begin{cases} \sqrt{2/3}[1 - \cos(2\pi t/T_c)] & t = [0, T_c] \\ 0 & otherwise \end{cases} \tag{37}$$

The ranging jitters of the above three waves can be defined as:

$$\sigma_{sq} = \frac{cT_c}{4}\frac{J_0(m_{RG})}{J_1(m_{RG})}\sqrt{\frac{B_L T_b}{2L_{ck}}\frac{1}{E_b/N_0}} \tag{38}$$

$$\sigma_{\sin} = \frac{cT_c}{4\sqrt{2}}\frac{J_0(m_{RG})}{J_1(m_{RG})}\sqrt{\frac{B_L T_b}{2L_{ck}}\frac{1}{E_b/N_0}} \tag{39}$$

$$\sigma_{tdrc} = \frac{cT_c}{8\sqrt{2/3}}\frac{J_0(m_{RG})}{J_1(m_{RG})}\sqrt{\frac{B_L T_b}{2L_{ck}}\frac{1}{E_b/N_0}} \tag{40}$$

According to equation (34), the ranging jitter σ is inversely proportional to the value of $h(T_c/2)$, which is the center peak of the ranging chip pulse. The ranging jitter can be reduced by increasing the center peak of the ranging chip pulse, to improve the system ranging accuracy. According to the above rationale, this paper designs a novel chip pulse based on the normally distributed wave (nd). In contrast to the random variable in the normal distribution, the designed chip pulse only represents a mathematical function, which can be defined as:

$$h_{nd}(t) = \begin{cases} \dfrac{A_{nd}}{\delta\sqrt{2\pi}}\exp\left(-\dfrac{(t/T_c - 1/2)^2}{2\delta^2}\right) & t = [0, T_c] \\ 0 & otherwise \end{cases} \tag{41}$$

where A_{nd} is the amplitude of the normally distributed wave and its value must be chosen to ensure that the power of the wave is equal to 1, and δ is the energy distribution index. The smaller the value of δ is, the more concentrated the energy in the center of the wave is, the higher the ranging chip pulse peak is, the larger $h(T_c/2)$ is and the higher the ranging accuracy is. Figure 6 shows the values of A_{nd} and $h(T_c/2)$ as a function of δ.

For the three traditional ranging chip pulses, the values of $h(T_c/2)$ can be calculated as 1, $\sqrt{2}$, and $2\sqrt{2/3}$ with equations (35) to (37). To obtain a larger value of $h(T_c/2)$, the maximum value of the energy distribution index is set to 0.2 according to Figure 6. On the other hand, the energy of the normally distributed wave will be concentrated near the peak when the energy distribution index is low, which may reduce the spectral efficiency of the composite signal. Considering the above factors, values of δ are selected as 0.2, 0.1 and 0.05 in this paper. Accordingly, the values of A_{nd} are 0.8422, 0.5954 and 0.4210, respectively, and the values of $h(T_c/2)$ are 1.6799, 2.3753 and 3.3591, respectively. Figure 7 shows the waveform of the above three cases (assuming T_c is 1). Other values can be selected according to specific requirements.

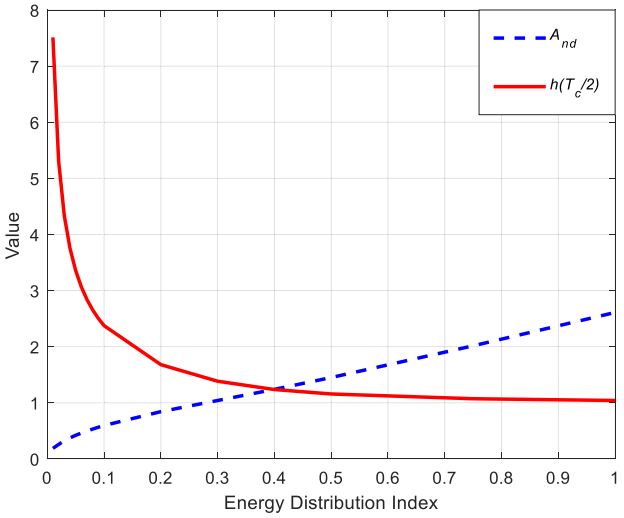

FIGURE 6. Variation diagram of the energy distribution index.

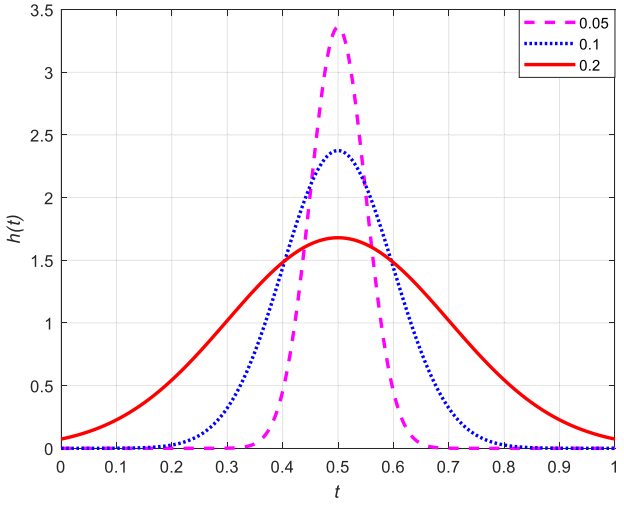

FIGURE 7. Normally distributed wave.

The ranging jitter of the above normally distributed waves can be expressed as:

$$\sigma_{nd-0.2} = \frac{cT_c}{6.72}\frac{J_0(m_{RG})}{J_1(m_{RG})}\sqrt{\frac{B_L T_b}{2L_{ck}}\frac{1}{E_b/N_0}} \tag{42}$$

$$\sigma_{nd-0.1} = \frac{cT_c}{9.50}\frac{J_0(m_{RG})}{J_1(m_{RG})}\sqrt{\frac{B_L T_b}{2L_{ck}}\frac{1}{E_b/N_0}} \tag{43}$$

$$\sigma_{nd-0.05} = \frac{cT_c}{13.44}\frac{J_0(m_{RG})}{J_1(m_{RG})}\sqrt{\frac{B_L T_b}{2L_{ck}}\frac{1}{E_b/N_0}} \tag{44}$$

It is clear that the ranging jitter decreases with decreasing energy distribution index of the normally distributed wave.

V. SIMULATION RESULTS AND ANALYSIS

In this section, the proposed normally distributed waves and three reference waves are simulated and analyzed. The simulation parameters are listed in Table 1.

TABLE 1. Simulation parameters.

Parameters	Values
Code length of the LDPC	1950 bits
Code rate of the LDPC	3/4
Encoding methods	Iterative encoding
Decoding method	Belief propagation decoding
Carrier frequency	6×1.023 MHz
Communication symbol rate	1.023 Ms/s
CPM modulation index	1/8
CPM M-ary	8
CPM shaping pulse	RC
Ranging modulation index	h=0.1 and 0.2
Ranging code	T2B and T4B
Ranging chip rate	3.069 Mchips/s
Sampling frequency	24×1.023 MHz
CTL bandwidth	1 Hz

A. SPECTRAL PERFORMANCE

Figure 8 to 11 show the spectral performance of the six chip pulses when T2B and T4B are selected for the ranging code and values of 0.1 and 0.2 are selected for the ranging modulation index, where "sq" is the square wave, "sin" represents the half-sine wave, "tdrc" indicates the time domain-rising cosine wave, "nd" is the proposed normally distributed wave, and 0.2, 0.1, and 0.05 are energy distribution index values.

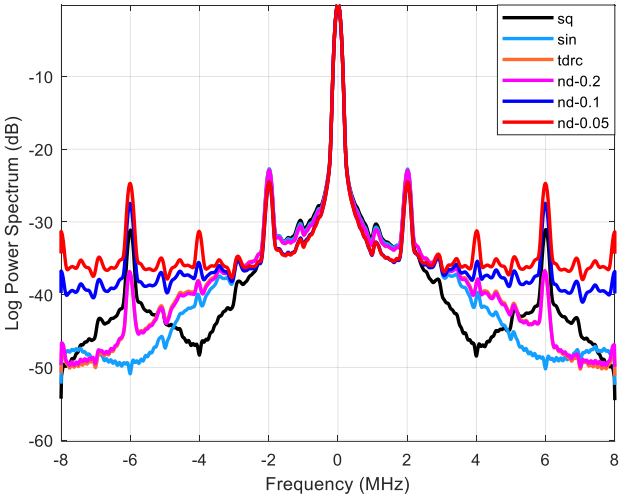

FIGURE 8. Power spectrum for T2B and h = 0.1.

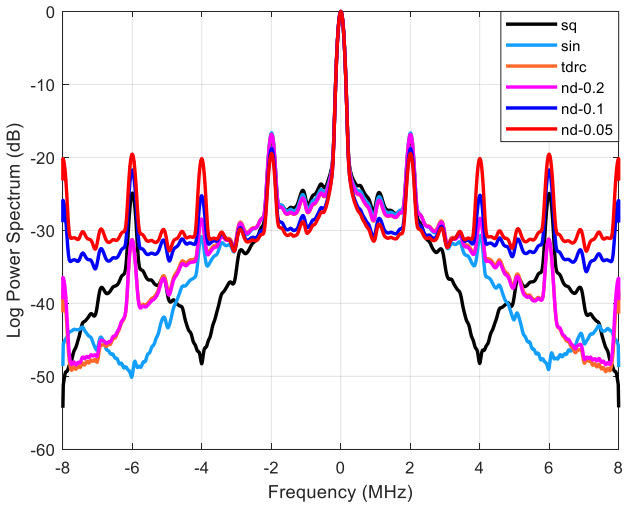

FIGURE 9. Power spectrum for T2B and h = 0.2.

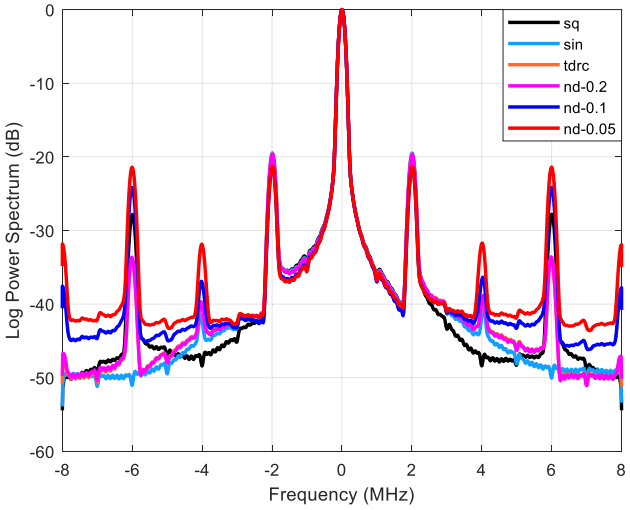

FIGURE 10. Power spectrum for T4B and h = 0.1.

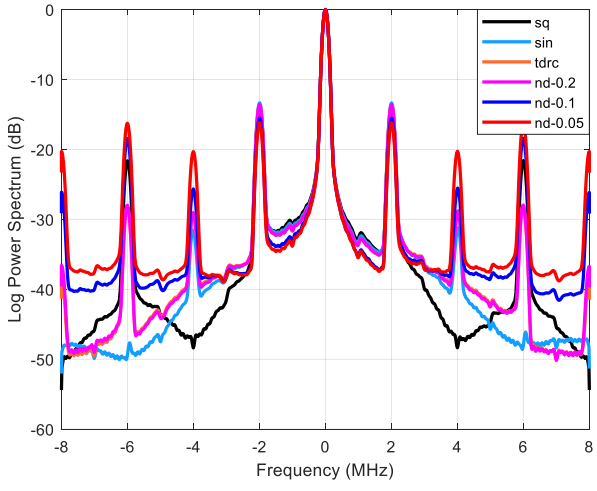

FIGURE 11. Power spectrum for T4B and h = 0.2.

It is observed that the square and half-sine waves attain a high bandwidth efficiency, while the spectral performance of the normally distributed wave is not ideal, especially when the energy distribution index is 0.05. The reason for this situation is that the energy of the normally distributed wave is concentrated near the peak when the energy distribution index

is low, thus resulting in multiple large side lobes in the composite signal spectrum. However, the spectral performance does not affect the communication reliability when the appropriate energy distribution index is chosen for the normally distributed wave (as shown in Figures 12-15). In addition, the parameters T2B and h = 0.1 exhibit a high spectral performance.

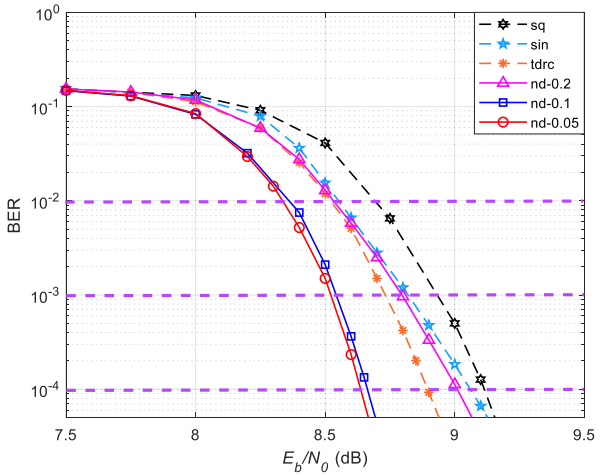

FIGURE 12. Communication BER for T2B and h = 0.1.

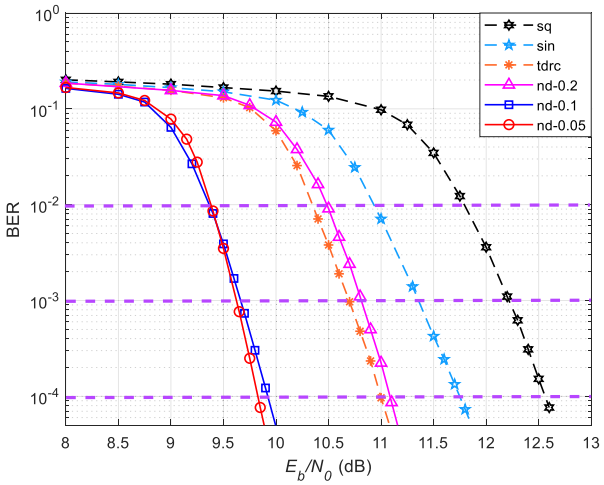

FIGURE 13. Communication BER for T2B and h = 0.2.

B. COMMUNICATION RELIABILITY

Figures 12 to 15 depict the communication reliability (in terms of the BER) of the six ranging chip pulses for the different parameters.

The above simulation figures reveal that the square and half-sine waves achieve a low BER performance, while the proposed normally distributed wave exhibits a great advantage when the energy distribution index is selected as 0.1 and 0.2. However, the normally distributed wave attains the worst performance regarding the error when the energy distribution index is 0.05 and the ranging code is T4B. This may have occurred because the energy of the ranging chip pulse is too

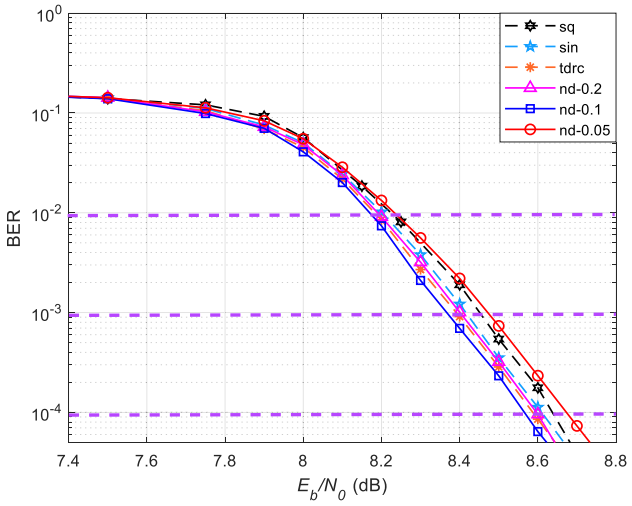

FIGURE 14. Communication BER for T4B and h = 0.1.

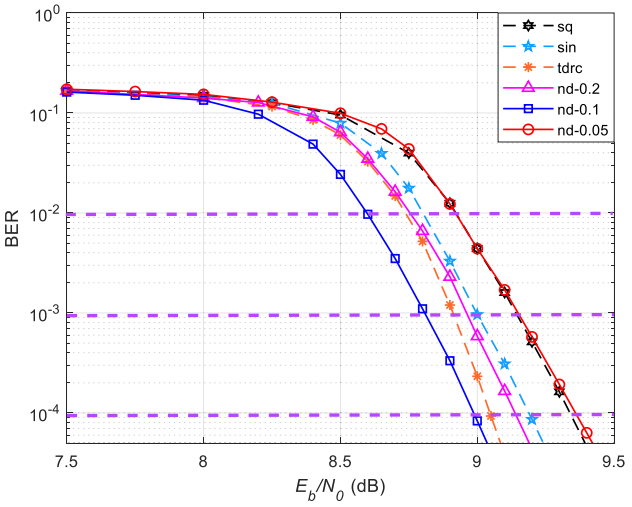

FIGURE 15. Communication BER for T4B and h = 0.2.

concentrated, which would lead to an enhanced interference of the communication signal. In addition, the effect of the different chip pulses on the communication performance is more notable when the ranging code is T2B or the ranging modulation index is high. In summary, the normally distributed wave presented in this paper attains a better communication performance than the other waves when the energy distribution index is between 0.1 and 0.2.

For comparison convenience, Tables 2 to 5 provide the required E_b/N_0 values (dB) for the six chip pulses to satisfy the target BER.

C. ACQUISITION TIME

The relationship between the acquisition time and E_b/N_0 (dB) can be obtained with equation (18), as shown in Figure 16.

The acquisition time of T2B is much smaller than that of T4B in the same channel environment, and it attains a higher performance when the ranging modulation index is high.

TABLE 2. E_b/N_0(dB) for T2B and h = 0.1.

Wave	E_b/N_0 (dB) for the Different Target BER		
	10^{-2}	10^{-3}	10^{-4}
sq	8.69	8.95	9.11
sin	8.55	8.81	9.06
tdrc	8.52	8.73	8.89
nd-0.2	8.53	8.80	9.01
nd-0.1	8.35	8.54	8.66
nd-0.05	8.33	8.52	8.63

TABLE 3. E_b/N_0 (dB) for T2B and h = 0.2.

Wave	E_b/N_0 (dB) for the Different Target BER		
	10^{-2}	10^{-3}	10^{-4}
sq	11.78	12.22	12.55
sin	10.92	11.35	11.76
tdrc	10.34	10.69	10.99
nd-0.2	10.48	10.81	11.08
nd-0.1	9.36	9.67	9.93
nd-0.05	9.38	9.65	9.84

TABLE 4. E_b/N_0 (dB) for T4B and h = 0.1.

Wave	E_b/N_0 (dB) for the Different Target BER		
	10^{-2}	10^{-3}	10^{-4}
sq	8.22	8.45	8.64
sin	8.20	8.42	8.61
tdrc	8.18	8.39	8.59
nd-0.2	8.19	8.40	8.60
nd-0.1	8.17	8.37	8.56
nd-0.05	8.23	8.47	8.67

TABLE 5. E_b/N_0 (dB) for T4B and h = 0.2.

Wave	E_b/N_0 (dB) for the Different Target BER		
	10^{-2}	10^{-3}	10^{-4}
sq	8.92	9.13	9.33
sin	8.80	8.99	9.18
tdrc	8.73	8.91	9.04
nd-0.2	8.75	8.96	9.13
nd-0.1	8.59	8.81	8.99
nd-0.05	8.92	9.14	9.35

When the target BER of communication is 10^{-2}, 10^{-3} and 10^{-4}, the acquisition time can be calculated, as summarized in Tables 6 to 9. The acquisition time of the various chip pulses is roughly the same for the different parameters (they differ at the 0.1 millisecond level among the different chip pulses). The main factor that impacts the acquisition time is the choice of the ranging code, and T2B attains a higher performance than T4B.

D. RANGING JITTER

The case of T2B and h = 0.1 is selected as a representative case (the other parameter conditions are similar) to illustrate the ranging jitter of the six chip pulses for different E_b/N_0 values (dB), as shown in Figure 17. The proposed normally distributed wave exhibits the lowest ranging jitter and the advantage becomes more notable when the channel conditions are poor.

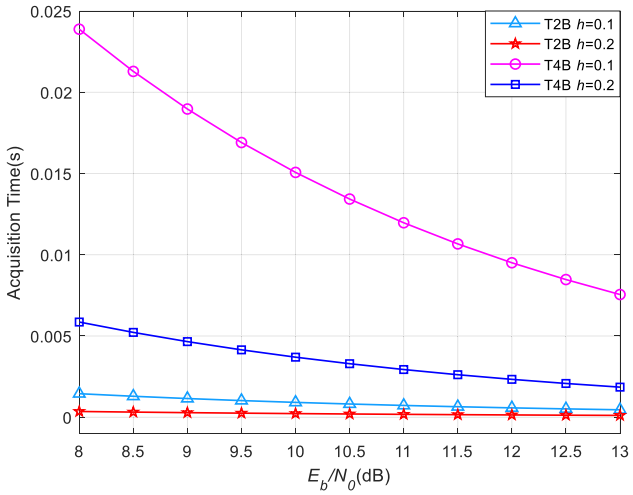

FIGURE 16. Acquisition time (s) for T2B, T4B and h = 0.1, h = 0.2.

TABLE 6. Acquisition time (ms) for T2B and h = 0.1.

Wave	Acquisition Time (ms) for the Different Target BER		
	10^{-2}	10^{-3}	10^{-4}
sq	1.2	1.2	1.1
sin	1.3	1.2	1.1
tdrc	1.3	1.2	1.2
nd-0.2	1.3	1.2	1.1
nd-0.1	1.3	1.3	1.2
nd-0.05	1.3	1.3	1.3

TABLE 7. Acquisition time (ms) for T2B and h = 0.2.

Wave	Acquisition Time (ms) for the Different Target BER		
	10^{-2}	10^{-3}	10^{-4}
sq	0.1	0.1	0.1
sin	0.2	0.2	0.1
tdrc	0.2	0.2	0.2
nd-0.2	0.2	0.2	0.2
nd-0.1	0.3	0.2	0.2
nd-0.05	0.3	0.2	0.2

TABLE 8. Acquisition time (ms) for T4B and h = 0.1.

Wave	Acquisition Time (ms) for the Different Target BER		
	10^{-2}	10^{-3}	10^{-4}
sq	22.7	21.5	20.6
sin	22.8	21.7	20.8
tdrc	22.9	21.8	20.8
nd-0.2	22.9	21.8	20.8
nd-0.1	23.0	21.9	21.0
nd-0.05	22.6	21.4	20.5

When the target BER of communication is 10^{-2}, 10^{-3} and 10^{-4}, the ranging jitter can be calculated, as summarized in Tables 10 to 13.

The normally distributed wave attains the smallest ranging jitter error, and the lower the energy distribution index is,

TABLE 9. Acquisition time (ms) for T4B and h = 0.2.

Wave	Acquisition Time (ms) for the Different Target BER		
	10^{-2}	10^{-3}	10^{-4}
sq	4.7	4.5	4.3
sin	4.9	4.7	4.5
tdrc	5.0	4.8	4.6
nd-0.2	4.9	4.7	4.5
nd-0.1	5.1	4.9	4.7
nd-0.05	4.7	4.5	4.3

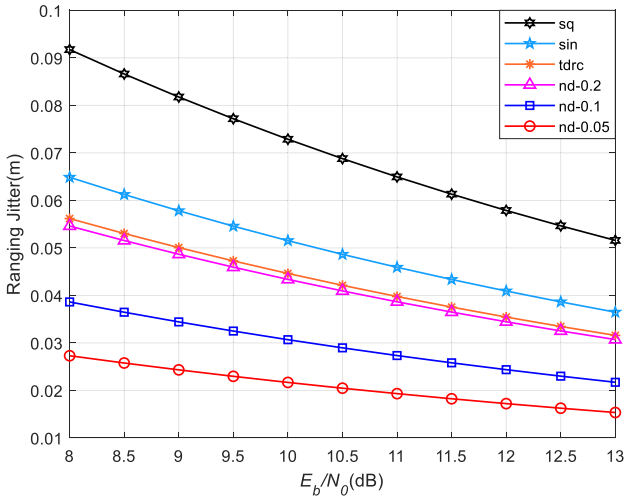

FIGURE 17. Ranging jitter (m) for T2B and h = 0.1.

TABLE 10. Ranging jitter (m) for T2B and h = 0.1.

Wave	Ranging Jitter (m) for the Different Target BER		
	10^{-2}	10^{-3}	10^{-4}
sq	0.0847	0.0822	0.0807
sin	0.0609	0.0591	0.0574
tdrc	0.0529	0.0517	0.0507
nd-0.2	0.0514	0.0498	0.0486
nd-0.1	0.0371	0.0363	0.0358
nd-0.05	0.0263	0.0257	0.0254

TABLE 11. Ranging jitter (m) for T2B and h = 0.2.

Wave	Ranging Jitter (m) for the Different Target BER		
	10^{-2}	10^{-3}	10^{-4}
sq	0.0294	0.0280	0.0269
sin	0.0230	0.0218	0.0208
tdrc	0.0213	0.0204	0.0197
nd-0.2	0.0203	0.0196	0.0190
nd-0.1	0.0164	0.0158	0.0153
nd-0.05	0.0115	0.0112	0.0109

TABLE 12. Ranging jitter (m) for T4B and h = 0.1.

Wave	Ranging Jitter (m) for the Different Target BER		
	10^{-2}	10^{-3}	10^{-4}
sq	0.0598	0.0582	0.0570
sin	0.0424	0.0413	0.0404
tdrc	0.0368	0.0359	0.0351
nd-0.2	0.0357	0.0349	0.0341
nd-0.1	0.0253	0.0247	0.0242
nd-0.05	0.0178	0.0173	0.0169

the smaller the ranging jitter is. In addition, the ranging jitter error is small when the ranging modulation index is high or when T4B is chosen as the ranging code.

TABLE 13. Ranging jitter (m) for T4B and h = 0.2.

Wave	Ranging Jitter (m) for the Different Target BER		
	10^{-2}	10^{-3}	10^{-4}
sq	0.0273	0.0267	0.0261
sin	0.0196	0.0192	0.0187
tdrc	0.0171	0.0167	0.0165
nd-0.2	0.0166	0.0162	0.0159
nd-0.1	0.0119	0.0117	0.0114
nd-0.05	0.0081	0.0079	0.0077

VI. CONCLUSION

The simultaneous transmission of communication and ranging information is an efficient transmission scheme for the ISLs of GNSSs. The main factors influencing the ranging accuracy of the CPM + PN scheme are analyzed in this paper, and a new ranging chip pulse based on the normally distributed wave is proposed. The simulation results show that the proposed normally distributed wave exhibits a great advantage in terms of the ranging jitter, which becomes more notable with decreasing energy distribution index. In terms of the acquisition time, the normally distributed waves achieve a similar performance to the traditional waves. In addition, the interference of the normally distributed wave to the communication signal is lower than that of the traditional waves, and the performance difference in communication reliability becomes more notable when the ranging modulation index is high. However, more energy is concentrated in the center of the wave when the energy distribution index of the proposed chip pulse is very low, which results in a low spectral efficiency. Considering the above factors, this paper suggests that the energy distribution index of the proposed normally distributed wave should be selected as approximately 0.1. In this case, the normally distributed wave exhibits great advantages in terms of the ranging accuracy and communication reliability.

REFERENCES

[1] J. Huang, W. Liu, Y. Su, and F. Wang, "Cascade optimization design of inter-satellite link enhanced with adaptability in future GNSS satellite networks," *GPS Solutions*, vol. 22, no. 2, p. 44, Feb. 2018.

[2] O. Luba, L. Boyd, A. Gower, and J. Crum, "GPS III system operations concepts," *IEEE Aerosp. Electron. Syst. Mag.*, vol. 20, no. 1, pp. 10–18, Jan. 2005.

[3] J. Chang, L. Shang, and G. Li, "The research on system error of Inter-satellite-link (ISL) measurements for autonomous navigation of beidou system," *Adv. Space Res.*, vol. 60, no. 1, pp. 65–81, Jul. 2017.

[4] Y. Xu, Q. Chang, and Z. Yu, "On new measurement and communication techniques of GNSS inter-satellite links," *Sci. China Technolog. Sci.*, vol. 55, no. 1, pp. 285–294, Jan. 2012.

[5] J. Huang, Y. Su, W. Liu, and F. Wang, "Adaptive modulation and coding techniques for global navigation satellite system inter-satellite communication based on the channel condition," *IET Commun.*, vol. 10, no. 16, pp. 2091–2095, Nov. 2016.

[6] D. Yang, J. Yang, G. Li, Y. Zhou, and C. Tang, "Globalization highlight: Orbit determination using BeiDou inter-satellite ranging measurements," *GPS Solutions*, vol. 21, no. 3, pp. 1395–1404, Apr. 2017.

[7] R. Xue, H. Yu, and Q. Cheng, "Adaptive coded modulation based on continuous phase modulation for inter-satellite links of global navigation satellite systems," *IEEE Access*, vol. 6, pp. 20652–20662, Apr. 2018.

[8] E. Vassallo and M. Visintin, "Analysis of UQPSK for simultaneous transmission of ranging and telemetry," in *Proc. SLSRFM. CCSDS Meeting*, Pasadena, CA, USA, 2009, pp. 132–137.

[9] *Efficient Spectrum Utilization for Space Science Services on Space-to-Earth Links*, CCSDS, Washington, DC, USA, 2014.
[10] R. S. Orr and D. Divsalar, "Combined GMSK modulation and PN ranging for communications and navigation," in *Proc. IEEE Aerosp. Conf.*, Mar. 2008, pp. 1–18.
[11] E. Vassallo and M. Visintin, "Analysis of GMSK for simultaneous transmission of ranging and telemetry," presented at the CCSDS Radio Freq. Modulation Workshop Group Meeting, Noordwijk, The Netherlands, 2009.
[12] E. Vassallo and M. Visintin, "Analysis of UQPSK and GMSK/PN for simultaneous transmission of ranging and telemetry: Ranging correlator results," in *Proc. CCSDS Radio Freq. Modulation Workshop. Group Meeting*, Portsmouth, VA, USA, 2010, pp. 243–250.
[13] E. Vassallo and M. Visintin, "GMSK and PN ranging: Combining option with improved spectral performance," presented at the CCSDS Radio Freq. Modulation Workshop Group Meeting, Portsmouth, VA, USA, 2010.
[14] R. S. Orr and D. Divsalar, "CPM/PN modulation and ranging for bandwidth-limited multiple access links," in *Proc. Aerosp. Conf.*, Mar. 2011, pp. 1–27.
[15] G. Sessler, E. Vassallo, and M. Visintin, "Performance of GMSK for telemetry and PN ranging under realistic conditions," in *Proc. 6th ESA Int. Workshop Tracking, Telemetry, Com-Mand Syst. Space Appl.*, Noordwijk, The Netherlands, 2013, pp. 1–8.
[16] F. Winterstein, "Simultaneous transmission of GMSK telemetry and PN ranging: Measurement report in support of the draft CCSDS recommendations 401(2.4.22A) and 401(2.4.22B)," presented at the CCSDS Radio Freq. Modulation Workshop Group Meeting, London, U.K., 2014.
[17] G. P. Calzolari, E. Vassallo, G. Sessler, and M. Visintin, "GMSK/PN for high rate telemetry and high accuracy ranging of Lagrange and mars missions," in *Proc. SpaceOps Conf.*, May 2014, p. 1851.
[18] G. Sessler and E. Vassallo, "GMSK and PN ranging: Improved telemetry signal demodulation using PN ranging signal cancellation," presented at the CCSDS Radio Freq. Modulation Workshop Group Meeting, San Antonio, TX, USA, 2017.
[19] B.-T. Peng, H. Ma, and K. Gao, "Mutual interference analysis of regenerative PN code ranging and telemetry," in *Proc. Int. Conf. Wireless Commun., Netw. Appl. WCNA*, 2017, pp. 24–29.
[20] R. Xue, Y. Cao, and T. Wang, "Data-aided and Non-Data-aided SNR estimators for CPM signals in ka-band satellite communications," *Information*, vol. 8, no. 3, p. 75, Jun. 2017.
[21] G. Kulikov and O. Belousov, "Multi-h CPM signal format selection for communication systems with complex jamming environment," in *Proc. Int. Conf. Eng. Telecommun.*, Nov. 2014, pp. 43–45.
[22] R. Xue, Q.-M. Cao, and Q. Wei, "A flexible modulation scheme design for C-Band GNSS signals," *Math. Problems Eng.*, vol. 2015, pp. 1–8, Jun. 2015.
[23] G. Cariolaro, T. Erseghe, N. Laurenti, and G. Pierobon, "New results on the spectral analysis of Multi-h CPM signals," *IEEE Trans. Commun.*, vol. 59, no. 7, pp. 1893–1903, Jul. 2011.
[24] L. Bing, T. Aulin, B. Bai, and H. Zhang, "Design and performance analysis of multiuser CPM with single user detection," *IEEE Trans. Wireless Commun.*, vol. 15, no. 6, pp. 4032–4044, Jun. 2016.
[25] R. Xue, Y. Sun, and D. Zhao, "CPM signals for satellite navigation in the s and c bands," *Sensors*, vol. 15, no. 6, pp. 13184–13200, Jun. 2015.
[26] D. Wang, R. Xue, and Y. Sun, "A ranging code based on the improved logistic map for future GNSS signals: Code design and performance evaluation," *EURASIP J. Wireless Commun. Netw.*, vol. 2017, no. 1, p. 57, Dec. 2017.
[27] R. Xue, Y. Xiong, and Q. Cheng, "A novel ranging code based on improved logistic map chaotic sequences," in *Proc. 21st Int. Conf. Adv. Commun. Technol. (ICACT)*, Feb. 2019, pp. 11–15.
[28] *Pseudo-Noise (PN) Ranging Systems, CCSDS 414.1-B-2*, Consultative Committee Space Data Syst., 2014.
[29] D. Lee, "Simulations of GMSK-PN and UQPSK," presented at the CCSDS Radio Freq. Modulation Workshop Group Meeting, Berlin, Germany, 2011.
[30] G. Sessler, M. Visintin, and E. Vassallo, "Analysis of GMSK/PN modulation: Effects of phase jumps and noise," presented at the CCSDS Radio Freq. Modulation Workshop Group Meeting, Boulder, CO, USA, 2011.
[31] G. Sessler, E. Vassallo, and M. Visintin, "Lagrange/Mars missions link budgets for GMSK and PN ranging," presented at the CCSDS Radio Freq. Modulation Workshop Group Meeting, Boulder, CO, USA, 2011.
[32] E. Vassallo and M. Visintin, "Synchronization analysis for GMSK/PN modulation," presented at the CCSDS Radio Freq. Modulation Workshop Group Meeting, Berlin, Germany, 2011.
[33] *Simultaneous Transmission of GMSK Telemetry and PN Ranging, CCSDS 413.1-G-1*, Consultative Committee Space Data Syst., 2017.

RUI XUE received the M.S. and Ph.D. degrees in communication engineering and information and communication engineering from Harbin Engineering University, Harbin, China, in 2006 and 2009, respectively. Since July 2003, he has been with the College of Information and Communication Engineering, Harbin Engineering University. From July 2011 to July 2012, he was an Academic Visitor with the Nonlinear Signal Processing Laboratory, University of Melbourne, Australia. He is currently an Associate Professor with the College of Information and Communication Engineering, Harbin Engineering University. His research interests include radio mobile communication systems, satellite communication systems, satellite navigation and positioning, error-correcting codes, high-spectral efficiency modulation, coded modulation, iterative decoding and detection, and so on.

TONG WANG received the B.E. degree in communication engineering from the Hebei University of Technology, Tianjin, China, in 2016. He is currently pursuing the Ph.D. degree in information and communication engineering with Harbin Engineering University, Harbin, China. His research interests include satellite communication, satellite navigation, adaptive transmission technology high-spectral efficiency modulation, and spread spectrum communication technology.

HUAIYU TANG received the M.S. degree in radio physics from the China Research Institute of Radiowave Propagation, Xinxiang, China, in 2009. He is currently pursuing the Ph.D. degree in military communications with Xidian University, Xi'an, China. He is also a Senior Engineer with the China Research Institute of Radiowave Propagation. His research interests include wireless self-organizing monitoring networks, electromagnetic spectrum monitoring, signal recognition and location technology, and so on.